ANALYSIS OF COMPOSITE MATERIALS VIA ELECTROMAGNETIC INVERSE SCATTERING

EYTAN BAROUCH

Department of Mechanical Engineering
Boston University, 110 Cummington St.
Boston, MA 02215, U.S.A.

Abstract

An extremely accurate forward and inverse scattering method has been developed and implemented for electromagnetic systems. This method is directly applicable for various real-time in-situ tasks. The forward scattering algorithm utilizes multipole "perfectly matched layer" boundary conditions as well as a complex realization of the permittivity functions of highly non-linear lossy materials, optimizing both storage and computational requirements. The method combines several hybrid components due to the inapplicability of typical inverse methods such as the conjugate gradient method and Hessian matrix inversion; these latter methods are inapplicable due to the hyperbolic nature of the Maxwell-material (MM) equations. Examples of highly structured inverse scattering of layered and structured objects that involve up to 23 independent parameters are given. The newly developed methodology as described and implemented herein is self-contained and can be modified to analyze various electromagnetic systems, regardless of scale, size and composition. The new method enables the accurate and efficient capture of effects of a broad variety of materials with various kinds of poles in the permittivity function that often occur with highly structured complex objects with multi-material lossy coatings.

1. Introduction

The quest for real-time in situ inverse scattering of complex two and three-dimensional objects composed of lossy materials coatings has been a major focus of the radar industry in part as a consequence of the developing technology of coating reflecting objects to act as non-reflecting ones. Other applications abound in the microchip industry [2] where the ever-decreasing scale size limits the applications of current technologies for metrology based

on electron microscopy. The basic requirement is an accurate and sufficiently fast algorithm so that real-time results are obtained efficiently.

This paper presents the development and implementation of a fast and accurate electromagnetic forward and inverse broad-band scattering algorithms, computing the scattered electromagnetic fields for all desired wavelengths simultaneously without sacrificing speed or accuracy. Two different inverse transform algorithms are employed. The first method involves the use of auxiliary differential equations for partial currents and the second method involves cumulative convolutions. The combination of these two unconventional techniques allows us to resolve the potential difficulty of non-unique solutions which is a result of the classic ill-posedness of inverse problems. In other words, we use the availability of two independent methods as a compatibility condition to yield a unique solution to the inverse problem. In the forward as well as the inverse transforms, the number of layers of the scattering objects is unrestricted.

In all cases, complex lossy materials can be used in which their analytical representation is obtained by a hybrid method that involves properties using material files that express the refractive index (N) and the absorption rate (K) as an explicit function of wavelength (WL) in nanometers (nm) or its energy in electron-volts (EV). The scattering process is essentially a continuous process requiring continuous representation of the material properties which is usually obtained as tables of N, K and wavelength (WL). Thus an optimization scheme has been developed using a three columns input file and returning an output of seven columns expressing the N, K, the real and imaginary reflectivities, the efficiency spectrum and the corresponding frequency. This method expresses each material as a sum of Debye-poles, Lorentz-poles, asymmetric Lorentz-poles (XLorentz-poles), conductivity term and plasma term as described by Lifshitz (ref. [5]) This method guarantees that causality holds in all cases. The ability to obtain real-time results depends on far field-near field transformations and 'perfectly matched layer' boundary conditions to minimize the computational domain whose limitations are well known (see, e.g., [1, 3, 8]).

2. Material Analysis

A typical material-file is expressed as a table of N and K as function of WL. The material properties of significance here are the real and imaginary parts of the permittivity and the efficiency spectrum (i.e., reflectivity) of a flat material. To obtain these properties for a given wavelength is elementary, so that if one wishes to develop numerical solutions for the Maxwell-Material (MM) equations [4] in the frequency domain a standard input file is sufficient. However, the computational cost associated with the MM equation per WL is large. If 200 spectral points are needed, the equations must be solved 200 times regardless of dimensions. Since accuracy depends primarily on the shortest wavelength, all equations are solved on the same grid, resulting in a very cumbersome and inefficient algorithm. On the other hand, the spatio-temporal MM equations provide the mechanism to obtain the scattered wave as a function of space and time, affording the computation of the scattered fields for all wavelengths using a novel non-uniform grid fast Fourier transform (FFT).

The development and implementation of the spatio-temporal MM equations requires delicate analysis. The material response to an external electromagnetic field is usually expressed in terms of the material polarization vector, which appears as a non-linear convolution with the electric field. If the material is also magnetic, a similar term involves the convolution of the magnetic permittivity with the magnetic field. In other words, to obtain scattering results with arbitrarily dense spectra we must be able to deal with more complicated equations whose entries are not easily available. Indeed, it is necessary to express the permittivity function as a continuous and differentiable function of the frequency.

In Paper I [2], it is explained how to do this while complying with basic physical principles, such as causality. The method involves judicious use of the "Lifshitz Integral" [5] which contains the permittivity function via dispersion relations. The result of this analysis is typically given in a form where three column input file of WL, N, K is first converted to a seven column input file of EV, N, K, RP, IP, Eff, QL, where RP, IP, Eff are the real and imaginary parts of the permittivity and Eff is the efficiency reflectivity. This detailed input file is inserted into the algorithm of inversion, changing the cost function for each iteration. The result is a material file specifying the number of poles in each term and the values of their corresponding

parameters. If one so wishes, the methodology employed here can yield uniform machine accuracy.

3. Perfectly Matched Layers

A method is also developed here for constructing perfectly matched layers (PMLs) for finite-difference time-domain (FDTD) computation (see [8]) that provides excellent impedance matches across a wide band of wavelengths. For both direct and inverse scattering computations, it is shown that perfectly matched layers provide the needed absorbed reflections over the required wide range of wave-lengths, so the computational domain may be decreased dramatically providing the ability for real-time analysis.

The requirement of a PML is that there will be no reflections as the wave enters the PML, or crosses from one PML layer to the next, whenever Berringer's transformations of impedance matching condition is satisfied [3]. A generalization of Berringer's approach for single lossy poles was introduced in [9]. It should be noted that in the case of periodic structures only one PML is being used in the bottom of the features and a thin layer of Silicon. In the case of isolated features five different PML are used, one on the bottom, one on each side of the computational domain and two in the intersecting corners. In all cases there is no PML imposed on the top of the domain since the reflected eave is the important outcome of the forward computation being fed into the inverse problem. Explicitly one obtains:

$$\frac{\mu + \dfrac{\sigma_d}{i\omega}}{\epsilon_d(\omega) + \dfrac{\sigma_d}{i\omega}} = \frac{\mu}{\epsilon(\omega)}, \tag{1}$$

where $\epsilon_d(\omega)$ and σ_d refer to the properties of a layer in the PML boundary. If $\epsilon(\omega)$ is a rational function, $\epsilon_d(\omega)$ will be also, and its structure computed. At $\omega = 0$,

$$\frac{\sigma_d}{\dfrac{\sigma_d^*}{\mu}} = \epsilon(0) = \epsilon_s \tag{2}$$

$$\sigma_d^* = \frac{\mu \sigma_d}{\epsilon_s}. \tag{3}$$

At $\omega = \infty$,

$$\epsilon_d(\infty) = \epsilon(\infty). \tag{4}$$

For $\omega \neq 0$, we solve for $\epsilon_d(\omega)$ and compare pole by pole (we are assuming that all poles are simple). If two functions are equal, all of their residues will be also:

$$\epsilon_d(\omega) = \epsilon(\omega)\left[1 + \frac{1}{i\omega}\frac{\sigma_d}{\epsilon_s}\right] - \frac{1}{i\omega}\sigma_d. \tag{5}$$

The Lorentz and X-Lorentz poles are at $\left\{\dfrac{s_k}{i}, \dfrac{s_k^*}{i}\right\}$

$$\text{Residue}\left\{\epsilon_d(\omega), \frac{s_k}{i}\right\} = \lim_{\omega \to \frac{s_k}{i}}\left(\omega - \frac{s_k}{i}\right)(\text{RHS}) \tag{6}$$

$$= \lim_{\omega \to \frac{s_k}{i}}\left(\omega - \frac{s_k}{i}\right)\epsilon(\omega)\left[1 + \frac{1}{i\omega}\frac{\sigma_d}{\epsilon_s}\right]$$

$$- \lim_{\omega \to \frac{s_k}{i}}\left(\omega - \frac{s_k}{i}\right)\frac{1}{i\omega}\sigma_d \tag{7}$$

$$= \text{Residue}\left\{\epsilon(\omega), \frac{s_k}{i}\right\}\left[1 + \frac{\sigma_d}{s_k\epsilon_s}\right], \tag{8}$$

so the s_k term of the computational domain permittivity is multiplied by the factor $\left[1 + \dfrac{\sigma_d}{s_k\epsilon_s}\right]$. The s_k^* term is handled similarly. Notice that if the term is a Lorentz pole, a_k is purely imaginary, but the above product is not. Therefore the Lorentz pole transforms to an X-Lorentz pole in the PML.

Since the Debye poles are located at $[\epsilon(\omega), -iv_{rj}]$, their residues are given by:

$$\text{Residue}\{\epsilon_d(\omega),\ -iv_{rj}\} = \lim_{\omega \to -iv_{rj}} (\omega + iv_{rj})(\text{RHS}) \qquad (9)$$

$$= \lim_{\omega \to -iv_{rj}} (\omega + iv_{rj})\,\epsilon(\omega)\left[1 + \frac{1}{i\omega}\frac{\sigma_d}{\epsilon_s}\right]$$

$$- \lim_{\omega \to -iv_{rj}} (\omega + iv_{rj})\frac{1}{i\omega}\,\sigma_d \qquad (10)$$

$$= \text{Residue}\{\epsilon(\omega),\ -iv_{rj}\}\left[1 + \frac{\sigma_d}{v_{rj}\epsilon_s}\right], \quad (11)$$

and so the coefficient of the Debye pole at $-iv_{rj}$ is multiplied by the factor $\left[1 + \dfrac{\sigma_d}{v_{rj}\epsilon_s}\right]$. The analysis for the poles located at $-iv_{rj}^*$ is analogous to analysis of the poles at $-iv_{rj}$.

Notice that if the term is a Lorentz pole, a_k is purely imaginary, but the above product is not. Therefore the Lorentz pole transforms to an *X*-Lorentz pole in the PML. In this paper a single PML layer is employed for the periodic case and 5 different PML layers are used for the isolated feature,

4. Numerical Methods

The spatio-temporal MM equations have been widely studied [4] and expressed in many forms [10]. Many algorithms have been devised to solve these equations for both general and specific purposes [6], with the fundamental conflicting issues being accuracy, speed and storage needs. Thus, to develop a forward scattering algorithm in two or three dimensions, one has to take these competing requirements into account based on end-user needs. A typical formulation of the MM equations is involves an integral equation representation which is particularly suitable for accurate solutions [10]. It is also most suitable to handle convolutions of permittivity functions with electric and magnetic fields. However, these integral equations usually require large storage due to fine grids since the system is hyperbolic in nature and much computing time since the matrices involved require direct inversions. Since most lithographic structures contain a SiO2 layer ranging from .4nm to 1nm thickness, a sub-.1nm grid is required to resolve this thin

SiO2 layer. In other words, even a 1000nm {*times*600nm 2D simulation requires a minimum of 10000 {*times*6000 grid points resulting in a long computation. To alleviate this difficulty, a number of studies include pre-computed libraries of forward scattering spectra, employing approximate algorithms for limited number of wavelengths, using multi-processors computers.

In this paper an alternative hybrid method is presented. A parameter file is constructed using the material files discussed above, using the various materials accordingly. The substrate can be decomposed into as many layers as needed, and the features share this property as well. The finest grid is near the circumference of the features, as well as at the very thin SiO2 layers needed. The finest grid used is one 15th of the lowest wavelength employed by the end user. In particular, the algorithm resolves 1nm with a 20nm grid when the lowest wavelength is 300nm. In a homogeneous domain of uniform composition the grids become coarser without loss of resolution using several non-uniform grid transforms to obtain the final computational grid. In 2D on a 3GHz single processor, the TE and TM polarization spectra are computed in 0.2-0.3 sec for as many wavelengths as one wishes. These computations are carried out for periodic as well as non-periodic systems and are applicable to reflectometry as well as ellipsometry measurements. The algorithm discussed here employs a non-uniform grid and it is applicable to 3D as well. It has been implemented in ANSI *C* and has been compiled on Solaris, Linux and Windows operating-systems, making it suitable for in-situ applications on many widely used systems.

As mentioned earlier, the main motivation for this study is to enable non-invasive reliable determination of composition and shapes of nano-features created during microlithography processing. The ultimate goal is the use of inverse scattering to determine the physical structure of materials having linear and non-linear permittivities, using an explicit FDTD [8] scheme, with updated coefficients for each time step; relatively simple applications are given below, while more complex applications will described in a third, follow-up paper. Good real-time performance of this software necessitates using a minimal computational domain. Since the substrate of silicon is huge compared with the size of features of interest (mm vs. nm), we use perfectly matched layer technology [1], while taking into account its potential pitfalls.

The measurements of the reflected waves describe both TM and TE polarizations of a broad-band spectrum of a few hundreds nanometers range. The features are described using connected trapezoidal structures which can be easily smoothed out by using by using bi-cubic splines. An optimization scheme similar to the one reported here is employed, and its most important parameters are the uppermost surface and the total height of the features. Each trapezoidal structure represents a single or a composite material, thus allowing us to obtain the shape and composition of the features [2]. It is mentioned here that to avoid the complication associated with trapezoidal corner, an optimal cubic-splines are use after every determination of the parameters. Here again the parameters are restricted as above to avoid the possibility of non-physical results.

The "cost" function in the actual execution of the inverse scattering engine is the length of the vector whose components are the difference between computed and measured reflected amplitude per measured wavelength, which is standard in scatterometry. The inverse problem has been treated as a combination of Brent formulation and multiple Newton methods. Each parameter is confined to a compact support domain assuring that all parameters are physically realistic. When the system wants to move a parameter outside of it prescribed support it moves back to the mirror image of its location with respect to the center of the "bell" function, given by:

$$B(x, a, b) = \sin\left\{\frac{\pi}{2}\int_{-\infty}^{x}\frac{1}{\epsilon\sqrt{2\pi}}\exp\left[\frac{[t-a]^2}{2\epsilon^2}\right]dt\right\} * \sin\left\{\frac{\pi}{2}\int_{x}^{\infty}\frac{1}{\epsilon\sqrt{2\pi}}\exp\left[\frac{[t-b]^2}{2\epsilon^2}\right]dt\right\}.$$

Note that the function $B(x, a, b)$ vanishes outside the interval $(a - \epsilon, b + \epsilon)$ thus providing a compact support for each function or number under this bell with ϵ being very small. When a parameter repeats attempting to exist the support domain, the parameter is fixed at its value corresponding to the lowest available cost function. In this study two tolerances are employed with values: Ftol = 0.001, Brenttoll = 0.00001. Due to the complex nature of the multi-materials features, the convergence rate is not uniform and feature dependent. The system is looking for a clear-cut direction to move and after some hovering makes a serious jump. After two or three of such steps both tollerances are met and the algorithm exits. It is displayed very explicitly in Figure 3-7.

The measured signal of amplitude per frequency is a function over compact support of the range of frequencies of interest. The measured signal is expanded in terms of two different bases within the "bell" function introduced by *Y.* Mayer (private communication). The signal is expressed in terms of the first basis, the largest components removed and then expanded in terms of the second basis and again the largest components removed. The remainder is noise. The sane operation is repeated with reversed order. The two remainders are averaged and are subtracted from the original signal. This simple procedure is very efficient in cleaning up signals. The spectra involved is finite in scope-200-800 nm wavelength. So the optimization scheme must be performed over compact support. The classical methods require each parameter to vary on the entire infinite domain which is definitely non-physical. The classic arctan map that can map the infinite domain to a finite domain presents serious difficulty. Some of the parameters are quite close to their allowed limits. Using the arctan map provides a zero-derivative and the parameter cannot move further. To alleviate this complication the system is expressed under a compact support "bell", assuring the ability of the parameters to move within the "bell" anywhere the system takes it. The observed signal is cleaned with a simple algorithm under the Bell -function and its noise is removed.

Explicitly one obtains:

$$E^{n+1} = \left(\frac{\epsilon_\infty - \xi^0}{\epsilon_\infty - \xi^0 + \chi^0} \right) E^n + \left(\frac{\Delta t / \epsilon_0}{\epsilon_\infty - \xi^0 + \chi^0} \right) \nabla \times H^{n+\frac{1}{2}} + \frac{\psi^n}{\epsilon_\infty - \xi^0 + \chi^0} \, , \quad (12)$$

where ψ^n is Luebbers "recursive accumulator", the sum of terms of the general recursive form given as:

$$\psi_p^n = \left(\Delta \chi_p^0 - \Delta \xi_p^0 \right) E^n + \Delta \xi_p^0 E^{n-1} + C_p^{\mathrm{rec}} \psi_p^{n-1} \qquad (13)$$

using

$$\chi^m = \int_{m\Delta t}^{(m+1)\Delta t} \chi(\tau) d\tau \qquad (14)$$

$$\xi^m = \int_{m\Delta t}^{(m+1)\Delta t} \xi(\tau)d\tau \tag{15}$$

only summed over all poles: Debye, Lorentz, and XLorentz.

$$\chi = \sum_{p \in \text{poles}} \chi_p \tag{16}$$

$$\xi = \sum_{p \in \text{poles}} \xi_p \tag{17}$$

$$\chi_p^m = \Delta\epsilon_p(1 - e^{-\Delta t/\tau_p})e^{-m\Delta t/\tau_p} \tag{18}$$

$$\xi_p^m = \frac{\Delta\epsilon_p\tau_p}{\Delta t}\left[1 - (\Delta t/\tau_p + 1)e^{-delt/\tau_p}\right]e^{-m\Delta t/\tau_p} \tag{19}$$

$$\Delta\chi_p^{m+1} = \Delta\chi_p^m e^{-\Delta t/\tau_p} \tag{20}$$

$$\Delta\xi_p^{m+1} = \Delta\xi_p^m e^{-\Delta t/\tau_p} \tag{21}$$

$$C_p^{\text{rec}} = e^{-\Delta t/\tau_p} \tag{22}$$

and for Lorentz poles, the expressions are complex, given explicitly as:

$$\hat{\chi}_p^m = \frac{-i\gamma_p}{\alpha_p - i\beta_p}\left[1 - e^{(-\alpha_p + i\beta_p)\Delta t}\right]e^{(-\alpha_p + i\beta_p)m\Delta t} \tag{23}$$

$$\hat{\xi}_p^m = \frac{-i\gamma_p/\Delta t}{(\alpha_p - i\beta_p)^2}\left\{[(\alpha_p - i\beta_p)\Delta t + 1]e^{(-\alpha_p + i\beta_p)m\Delta t} - 1\right\}e^{(-\alpha_p + i\beta_p)m\Delta t} \tag{24}$$

$$C_p^{\text{rec}} = e^{(-\alpha_p + i\beta_p)\Delta t}. \tag{25}$$

Only the real part of $\hat{\xi}_p^m$ is being used to update the E-field.

5. Forward and Inverse Scattering

In Figure 1 the continuous properties of crystalline Silicon are given. The left figure displays the efficiency spectrum of crystalline Silicon slab, the middle figure exhibits the continuous N and K as obtained from the

mentioned optimization algorithm and the right figure displays the real and imaginary parts of the reflected wave from the Silicon slab, All graphs are continuous functions of the wavelength.
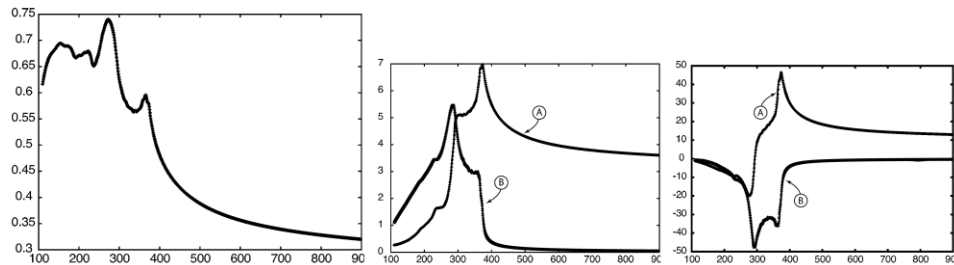

Figure 1. Efficiency, real and imaginary permittivity and reflected field of crystalline Silicon.

To illustrate the resolving power of the forward scattering methodology presented here, an example of a 10nm pitch of pure silicon grating of 500nm depth is given Figure 2, displaying the TM, TE and unpolarized efficiency reflection spectra.
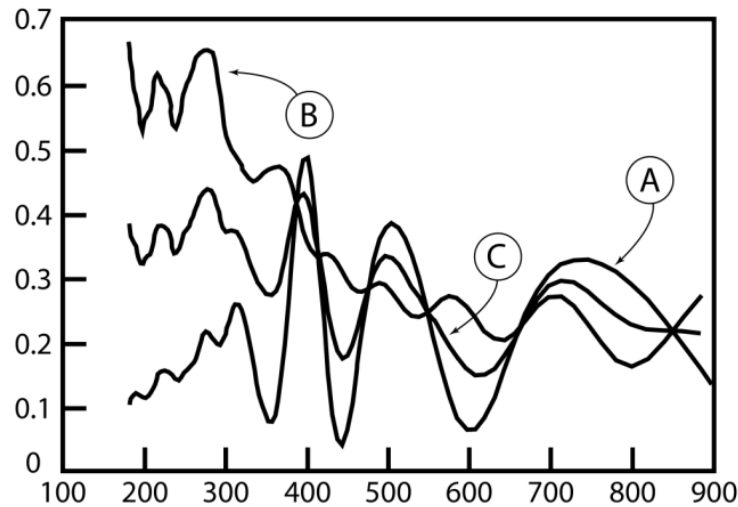
Figure 2. Efficiency spectra (dimensionless) vs. wavelength (in nm) of the grating for TM(A), TE(B) and unpolarized (C) fields.

The difficulties associated with inverse problems are well known, particularly for hyperbolic systems such as the MM equations. A general

analytical and numerical treatment of existence and uniqueness of solutions of ill-posed problems is an immense task. However, in applied inverse scattering, existence is certain but uniqueness is not. So one must formulate a system with guaranteed existence and examine all relevant solution within a narrow range of relevance such as CD control and projectile shapes. In most inverse problems, after the various compatibility conditions are constructed, partial derivatives with respect to the relevant parameters are needed. Numerical differentiation appears at first to be the only available tool, leading in some cases to totally wrong answers.

This paper employs a newly developed and implemented idea, bypassing the difficulties of numerical differentiation and non-uniqueness combined. After the initial guess is introduced, a series of coordinate affinic transformations take place, for each of several relevant cost functions. Several estimated Hessians are constructed together with their conjugate vector sets. The system so constructed is 'self-taught' and keeps updating itself until it reaches the prescribed tolerance and exits. As the Hessians get updated a second tolerance array invokes a second inverse algorithm with cubic convergence compared with the slower quadratic convergence rate. This split can be imposed at any stage with the understanding that the possibility of a non-unique solution will be detected as a result of the varying convergence rate. This methodology is heavily related to the forward scattering algorithm. It should be noted here that not all non-unique solutions are necessarily bad, since the main goal is to predict the feature shape and composition. As an example consider a trapezium shape described by three trapezia. The upper and lower CD and the feature height describe the uniquely, but the other four parameters can vary without affecting the final outcome (as long as the trapezium shape is preserved).

Several examples are given below with increasing complexity. In all of these examples, there is a common display order, viz., the initial guess, the final match and the target feature which is the desired one. Following the feature display, the efficiency spectra of the initial, intermediate, final and target are displayed. In most cases, the spectra employed is the unpolarized spectra determined by averaging the TE and TM polarizations, which are always computed by the forward scattering algorithm. In all examples here the substrate is composed of four layers. These layers are given in ascending

order as: 1. Silicon substrate, 2. Gate oxide SiO2 of 1.4nm thickness, 3. Polysilicon of 120nm thickness and 4. ARC SiON of 20nm. The photoresist is allowed to change between 50nm-350nm. In these example the substrate layers' thickness is kept fixed while all feature parameters are allowed to vary freely. In Figure 3 and Figure 4 the case of seven parameters feature is displayed. In Figure 3 the initial, final and target spectra are displayed. As can be clearly seen, each target point is matched by the final spectral points, while the initial spectrum is distinctly different. In Figure 4 the actual features are exhibited, according to the same order recipe of "first, final, target". In Figures 5-8, a 23-parameter feature is exhibited in the same order. Note that although the substrate is not displayed, it is an integral part of all computations.
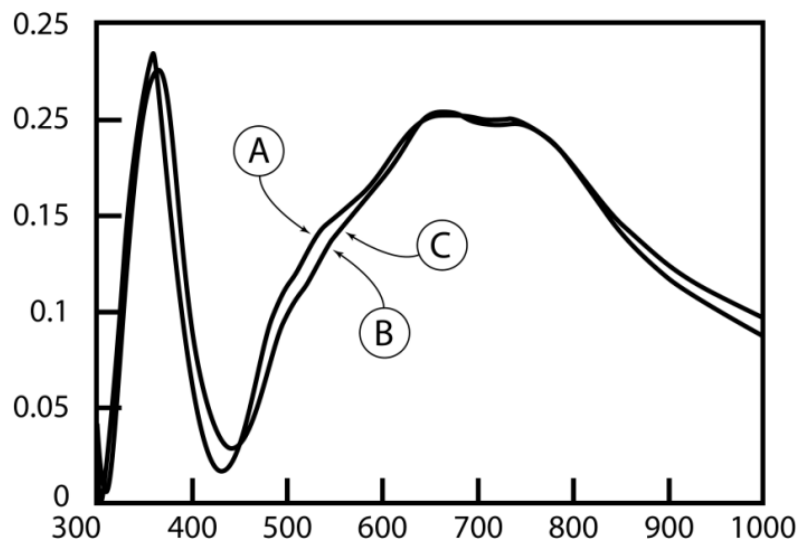
Figure 3. A comparison of the spectra of 7 parameters feature composed of three trapezoid, displaying the initial starting spectrum (A), the final spectrum (B) and the target spectrum (C). As can be clearly seen, (B) and (C) are indistinguishable.
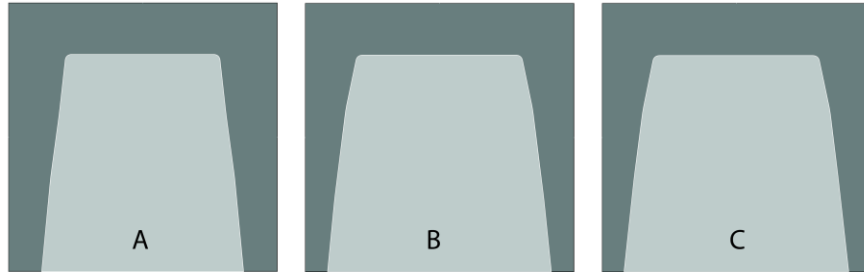
Figure 4. The actual shapes of the features composed of 3 trapezoid (7-parameters) of the inverse scattering process. These are the initial (A), final (B)and the actual target (C). Note that again (B) and (C) are indistinguishable.
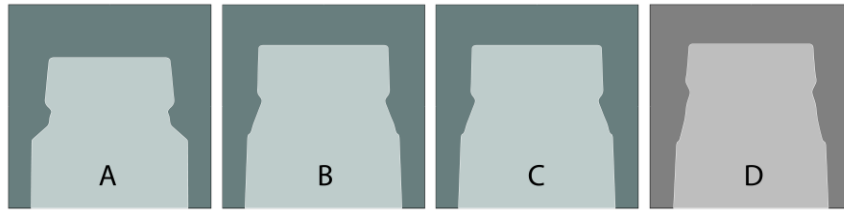

Figure 5. An inverse-scattering display of the initial (A), intermediate (B), final (C) and target (D) of the 23 parameters feature expressed as 11 trapezoid. Note that again (C) and (D) are indistinguishable.
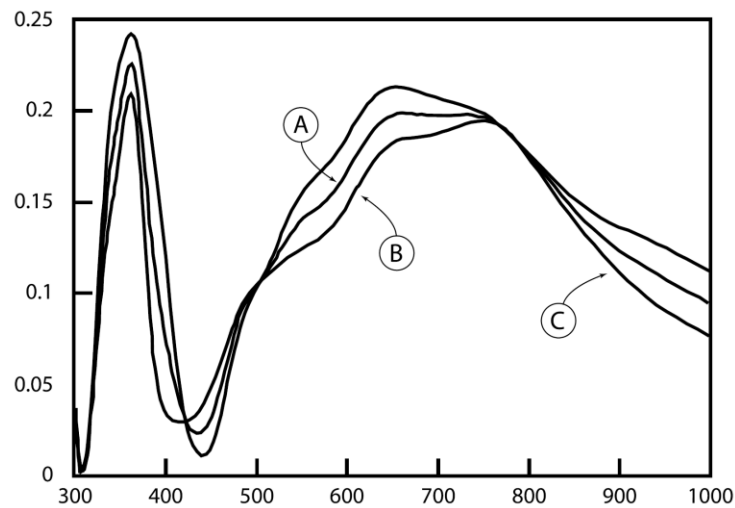

Figure 6. A plot of the final spectra (dimensionless) vs. wavelength (in nm) of the TM polarization (A), TE polarization (B) and the unpolarized (C) spectra of the 23 parameters feature. All dimensionless spectra are plotted vs. wavelength (in nm).
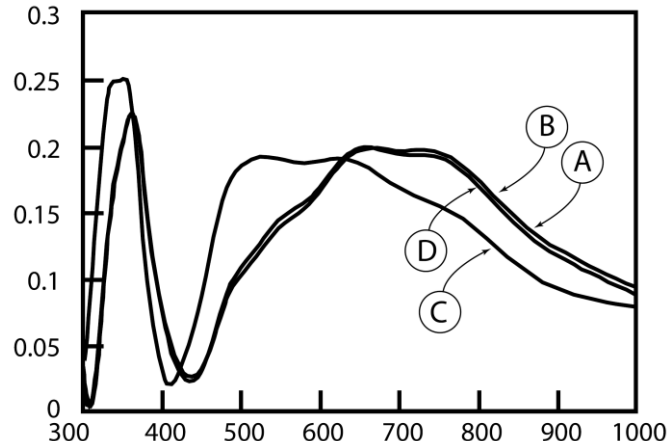
Figure 7. The reflection efficiency spectra of the inverse scattering process of the 23 parameters feature. The spectra of the initial (A), intermediate (B), final (C), and the target (D) are plotted (dimensionless) vs. wavelength (in nm).
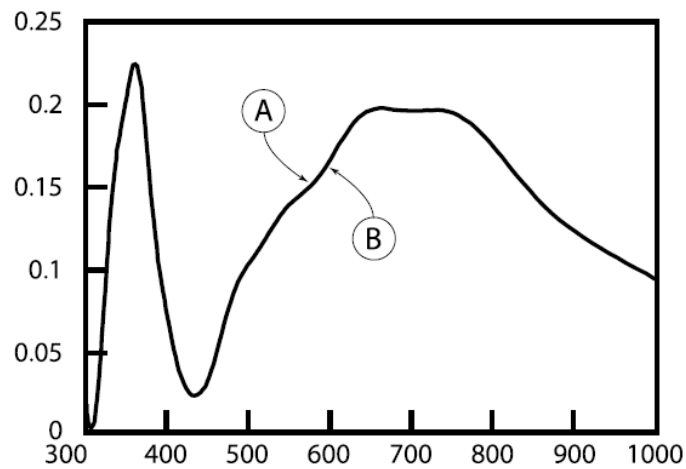

Figure 8. A comparison of the final unpolarized efficiency spectrum (A) with the target efficiency unpolarized spectrum (B). As can be seen they are indistinguishable and agree to machine accuracy.

6. Conclusions

A very fast and accurate forward and inverse scattering algorithms as well as complicated lossy material analysis methodology have been presented.

The speed, accuracy and flexibility of the system presented here, demonstrates its ability to perform in-situ metrology analysis in real-time on manufacturing IC lines and electromagnetic problems at other scales, such as radar.

Acknowledgment

References

[1]   S. Abarbanel, D. Gottlieb and J. S. Hesthaven, Long time behavior of the perfectly matched layer equations in computational electromagnetic, Journal of Scientific Computing 17(1-4) (2002), 405-422

[2]   E. Barouch and S. A. Orszag, Source optimization in optical lithography, Studies in Applied Mathematics 128(2) (2012), 144-158

[3]   J. P. Berringer, A perfectly matched Layer for the absorption of electromagnetic waves, J. Computational Physics 114 (1994), 185-200.

[4]   M. Born and E. Wolf, Principles of Optics, Pergamon Press, Sixth edition, 1987.

[5]   E. M. Lifshitz, The theory of molecular attractive forces between solids, Soviet Physics 2 (1956), 73-83.

[6]   D. Maystre, Integral methods, in Electromagnetic Theory of Gratings, R. Petit, Ed., Springer Verlag, 1980.

[7]   F. Pinto, Engine cycle of an optically controlled vacuum energy transducer, Physical Review B 60 (1999), 14740-14755.

[8]   A. Taflove and S. Hagness, Computational Electrodynamics: The Finite-Difference Time-Domain Method, Artech House, 2nd edition, 2000.

[9]   Toru Uno, Yiwei He and Saburo Adachi, Perfectly matched layer absorbing boundary condition for dispersive medium, IEEE Microwave and Guided Wave Letters 7(9) (1997), 264-266.

[10] M. S. Yeung and E. Barouch, Three-dimensional mask transmission simulation using a single integral equation method, Proc. SPIE 3334 (1998), 704-713.